Simulation of Etching in Chlorine Discharges Using an Integrated Feature Evolution-Plasma Model

Helen H. Hwang[a], Deepak Bose[b], T. R. Govindan, and M. Meyyappan
NASA Ames Research Center
Moffett Field, CA 94035 USA

Abstract

Etching of semiconductor materials is reliant on plasma properties. Quantities such as ion and neutral fluxes, both in magnitude and in direction, are often determined by reactor geometry (height, radius, position of the coils, etc.). In order to obtain accurate etching profiles, one must also model the plasma as a whole to obtain local fluxes and distributions. We have developed a set of three models that simulates Cl_2 plasmas for etching of silicon, ion and neutral trajectories in the plasma, and feature profile evolution. We have found that the location of the peak in the ion densities in the reactor plays a major role in determining etching uniformity across the wafer. For a stove top coil inductively coupled plasma (ICP), the ion density is peaked at the top of the reactor. This leads to nearly uniform neutral and ion fluxes across the wafer. A side coil configuration causes the ion density, as well as the ion fluxes, to peak near the sidewalls, which leads to substantial variations in etch profiles from the central to near-edge wafer regions. In addition, the ions bombard the wafer at a slight angle. This angle is sufficient to cause skewed profiles, which is highly undesirable.

[a] Electronic mail: hwang@dm1.arc.nasa.gov

[b] Eloret Corporation

I. Introduction

The evolution of etching profiles due to plasma processing conditions is of continuing concern in the semiconductor industry. It is critical to achieve an anisotropic etch to achieve straight walls in trenches, especially as linewidths are decreasing to 0.1 μm. Processing variables, such as gas pressure, rf bias voltage, and coil power, control the plasma properties (species densities, fluxes, electric fields, etc.). Differences in processing conditions, as well as in reactor geometries, have been observed to have dramatic impact on the resulting etch profiles on the substrate.[1,2] Although semi-analytic models can estimate etch rates and species fluxes to the wafer reasonably well,[3] any asymmetry that may arise due to processing or geometry concerns will not be captured. In particular, etch profile variation across the wafer cannot be resolved without calculating the differences in ion and neutral fluxes with respect to radial location.

In order to demonstrate the effects of the plasma on etched features, a feature profile evolution model would have to also consider the plasma properties, such as species fluxes, distributions with respect to impact angle of species landing on the wafer, etc. We have developed a suite of models that couples a plasma simulation to a feature profile evolution model via a third simulation which calculates trajectories of ions and neutral species landing on the wafer. The plasma simulation calculates variables such as electric fields, species densities, and average fluxes, which are then used by the Particle-in-Cell (PIC) simulation. The trajectories of ions and neutrals are advanced, generating velocity and angular distributions at specified locations on the wafer. The feature profile simulation uses the normalized distribution functions to calculate the fluxes and etch rate at any given point on the trench.

In this study, we consider chlorine etching of silicon, as chlorine gas mixtures are frequently used due to fast etch rates. The chlorine etch mechanism has been studied

extensively[4,5,6] and ion enhanced etch yields have been calculated and measured.[7,8,9] One observed phenomena that happens is microtrenching, or enhanced etching in the trench corners. Microtrenching is thought to occur due to grazing ions impacting the bowed sidewalls and reflecting off onto the trench bottoms as hot neutrals, thereby increasing the etch rate in the corners. However, microtrenching is not generally observed in shallow trenches and occurs only during the later portion of etching for high aspect ratio features.[10] For the sample features considered in this study, the aspect ratios are sufficiently small to neglect microtrenching.

II. Description of the Model

1. Semiconductor Equipment Modeling Software (SEMS)

Reactor scale modeling is handled by the Semiconductor Equipment Modeling Software, or SEMS. The SEMS code has been described elsewhere[11] and will briefly be described below. SEMS is 2-D in (r, z) and solves the appropriate fluid equations for all species using a finite difference, implicit Gauss-Seidel line relaxation scheme. Mass balance equations are solved for electrons, ions and neutrals, the energy balance equation for electrons, and Maxwell's equations for power coupling. Also included for the species is a self-consistent effective binary diffusion calculation. Bulk fluxes to the wafer are generated which are later used to normalize distribution functions calculated by the PIC simulation.

2. Particle-in-Cell Neutral and Ion Computation (PICNIC)

Since SEMS is a fluid model, the quantities that are calculated are averages (moments of the Boltzmann distribution function). However, the calculation of etch rates on the wafer depends on the angular information of impacting species in two ways. First, the etch yield is

dependent on the ion's impacting angle.[9,12] Second, the view factor, or the allowable range of angles for impacting species inside a feature, determines the fluxes of species to a particular point on the trench. Therefore, both velocity and angular distribution functions for species landing on the wafer are required, but these cannot be generated using SEMS. SEMS can only provide quantities such as average fluxes to the wafer, and not angle-dependent fluxes to the wafer. Hence, we have developed a separate, offline simulation to calculate these necessary distribution functions. The Particle-in-Cell Neutral and Ion Computation (PICNIC) calculates neutral and ion trajectories in the entire plasma reactor using bulk plasma quantities generated by SEMS (*e.g.*, species densities, electron temperature, electric fields). Although PICNIC is fully 3-D in both velocity and space, particle motion is restricted to 2-D in (r, z) in the present study. Restricting the motion of the particles ensures axisymmetric flow and therefore consistency with the calculations of SEMS. PICNIC calculates ion and neutral trajectories in the following manner. Particles are generated throughout the reactor according to electron-impact source rate functions from SEMS. Particles are generated with an initial Maxwellian velocity distribution, as there is no gas flow in the PICNIC calculation. Particle motion is tracked, assuming ions are accelerated by electric fields (generated from SEMS) and that both ions and neutrals suffer collisions. Electric fields are not computed self-consistently since electrons trajectories are not followed. The heavy species collisions are handled using a null-collision cross section method with velocity-dependent cross sections (see Hwang and Kushner[13]). Both momentum transfer and species altering collisions (*e.g.*, charge exchange, neutralization reactions) are allowed to occur. These collisions are treated differently from direction simulation Monte Carlo (DSMC), in that the particles do not collide with other particles in the simulation. Rather, the particles collide with a "fluid" background (based on the densities derived from SEMS) in a particle-mesh

fashion. Neutrals are allowed to collide at the wall and are reemitted as a new species (due to recombination) with a probability of $(1 - S_n)$, where S_n is the sticking coefficient. All particles retain their original velocity magnitudes and are reemitted from a cosine angular distribution. Cl is assumed to have a sticking coefficient of 0.1 in both SEMS and PICNIC.[14] Cl_2 has a sticking coefficient of zero, but can be removed from the simulation in the reactor at a loss rate determined by the electron impact source (loss) rate. Both Cl and Cl_2 can form $SiCl_x$ on the wafer in PICNIC and thus are removed from the simulation, as these trace species are not followed. Ions are assumed to have unity sticking coefficients at the walls and therefore are removed from the simulation once they encounter a wall. Because the sheaths are assumed to be thin in an ICP (much smaller than the mean free path), PICNIC assumes that the sheaths are collisionless and that all ions gain energy due to the sheath potential. SEMS calculates electric fields up to the presheath boundary, but not in the sheath itself. Therefore the ions must gain an additional amount of energy while falling through the sheath. For ions landing on the wafer, this gained energy results in a gain of velocity in the axial direction:[15]

$$\varepsilon_z = T_e \ln\left(\frac{M_i}{2\pi m_e}\right)^{1/2}, \text{ and} \qquad [1]$$

$$|v_z|_{\text{gain}} = \sqrt{\frac{2\varepsilon_z}{M_i}}, \qquad [2]$$

where T_e is the electron temperature, and M_i and m_e are the ion and electron masses, respectively.

The trajectories of ions in the plasma use electric fields generated by SEMS, ignoring the acceleration due to the azimuthal component. Statistics of species are collected at specified points on the wafer. Note that since the reactor is considered to be axisymmetric, all points at the same radial position have the same distribution function. This approach is similar to that of

Hoekstra and Kushner,[16] with the following differences. PICNIC calculates one distribution function for each neutral and ion species that bombard the wafer at each specified point based on impacting particle velocity and angle relative to the surface. The velocity used for the distribution function is actually the particle's velocity magnitude, or speed. Each distribution function at a point is thus 2-D in nature and is not the product of two separate distributions ($f(|v|,\theta)$ vs. $f(|v|)\cdot f(\theta)$). When collecting statistics at a particular point on the wafer, the trench alignment is assumed to be in the (r, z) plane. These distribution functions that are calculated are capable of capturing any angular asymmetry that may exist. However, this method does increase the computation time. Collecting statistics for a 2-D resolved distribution function requires on the order of 10,000 particles for 1000 iterations. The other difference in methodology from that of Ref. 16 is that PICNIC does not calculate species densities but relies upon values computed from SEMS.

3. Simulation of Profile Evolution using Level Sets (SPELS)

At a particular radial location on the wafer, the fluxes to the trench can be obtained using the velocity and angular distribution functions from PICNIC. We have developed a feature profile evolution simulation, SPELS, which has been described earlier.[17] The simulation approach has also been validated with experimental data for etching of high aspect ratio features in silicon using HBr[18]. Here we will provide a brief summary of the approach we use to calculate trench etching. SPELS uses a level set method to track the evolving surface.[19] Therefore, a "flux" must be calculated at each point in the 2-D (x, y) computational domain around the trench. The directed velocity (of either ion or neutral) has the form $|v|\cos(\theta-\xi)$, where $|v|$ is the magnitude

of the total velocity, θ is the impacting angle from the normal, and ξ is the angle of the surface from the normal (see Fig. 1). The impacting angle is defined as

$$\theta = \tan^{-1}\left(\frac{v_r}{v_z}\right). \qquad [3]$$

Then the directed flux from the plasma to a point on the surface is

$$\Gamma_{\text{plasma}} = \int_{\theta_1}^{\theta_2}\int_{0}^{v_{\max}} |v|\cos(\theta-\psi)\cdot f(|v|,\theta)\cdot|v|\, d|v|\, d\theta\,. \qquad [4]$$

Note that Eq. 4 does not include re-emission fluxes from the trench surface. Both ion and neutral fluxes are calculated according to Eq. 4 for each species. The net ion flux is summed over all ion species (Cl^+ and Cl_2^+), and the neutral flux is calculated from the sum of the fluxes of Cl and Cl_2. Re-emission fluxes for neutrals are accomplished using a line-of-sight calculation along the trench. Ion re-emission fluxes are ignored. Assuming that both molecular and atomic chlorine passivate the surface of the substrate and the ions etch the silicon chlorides, the etch rate can be obtained. We know that the chlorinated surface coverage at each point is[17]

$$\alpha(x,y) = \frac{S_{n0}\Gamma_n(x,y)}{S_{n0}\Gamma_n(x,y) + Y_{Cl}\Gamma_i(x,y)}, \qquad [5]$$

where S_{n0} is the neutral sticking probability, and Y_{Cl} is the Cl removal yield. Both Cl and Cl_2 are assumed to have the same sticking coefficient. This sticking coefficient refers to Cl and Cl_2 reacting with silicon and is different from the sticking coefficients mentioned in Section II.2,

which are recombination probabilities at the wall. The one exception is the sticking coefficient (reaction probability) of Cl and Cl_2 with Si at the wafer location in PICNIC. The etch rate *ER* at each point is then

$$ER = \frac{1}{\rho_{Si}} \cdot Y_{Si}(x,y) \cdot \Gamma_i(x,y) \cdot \alpha(x,y), \qquad [6]$$

where ρ_{Si} is the mass density of Si and Y_{Si} is the Si etch yield. According to Chang and Sawin[9], the etch yield is assumed to scale as

$$Y_{Si} = A\left(\sqrt{E_{ion}} - \sqrt{E_{th}}\right) \cdot Y(\theta), \qquad [7]$$

where A is a constant, E_{ion} is the ion's impact energy, and E_{th} = 10 eV. Thus, for relatively low sheath potentials of ~20 eV, the etch yield is of order A. The angular dependence $Y(\theta)$ is also given in Ref. 9 and is used for these cases.

The level set equation is used to advance a higher order variable $G(x, y, t)$, in which the plasma-surface interface occurs at $G(x, y, t_0) = 0$, or the zero level set. On the interface, the etch rate is equal to the opposite of the speed (S) of G. In the remaining (x, y) domain, G is updated by solving the level set equation,

$$\frac{dG}{dt} + S|\nabla G| = 0. \qquad [8]$$

Therefore, the trench movement is indirectly tracked as G is advanced. The simulation continues for a user-specified time.

III. Results and Discussion

For the following cases, the conditions given below are assumed for both SEMS and PICNIC. The reactor is a standard ICP 300 mm etch tool. Although we do not consider an additional rf bias on the substrate, an applied bias is typically used in order to increase the ion energy and thus increase the overall yield and etch rate. The increased bias has other benefits, as it will cause the ions to be accelerated primarily head-on to the wafer and thus reduce any skew in the presheath fields. A large applied rf bias also has been shown to decrease microtrenching.[1] However, low energy ion-assisted etch does exist in the range 20-50 eV and without an applied rf bias,[9,20] and hence the present simulations do represent practical cases of interest. Future studies will self-consistently include the effects of rf bias in SEMS as well as in PICNIC. Two configurations, with either a stove top or side coil, are considered. Both reactor configurations use chlorine gas at 10 mTorr, 500 W of ICP power, and gas temperature of 500 K. The electron-impact gas collisions are given in Table 1.[21] The heavy particle reactions that are considered in PICNIC are given in Table 2.

The densities of Cl_2^+ and Cl^+ are shown for the two coil configurations in Figs. 2 and 3. The peak ion densities should occur close to the coils due to the high amount of ionization. For the stove top coil case, both ion densities are peaked near the top of the reactor close to the coils, as shown in Fig. 2. The peak occurs mid-reactor, at a radial location around 12 to 14 cm. Thus, the maximum ion flux to the wafer should occur at approximately this same radial location because the ion velocities will not have a strong radial dependence. The maximum Cl^+ density is about 1.6 times that of the maximum density of Cl_2^+ (6.1×10^{10} cm^{-3} vs. 3.7×10^{10} cm^{-3}). For the side coil case, again the ion densities peak near the coil (see Fig. 3). The peaks of the ion densities occur close to the side walls at a radial location of approximately 20 cm. Again, one would expect maximum ion fluxes to the wafer at large radii, with decreasing ion fluxes at

locations closer to the reactor's axis of symmetry. The peak ion densities for Cl^+ and Cl_2^+ are comparable at about 5.6×10^{10} cm^{-3}.

The bulk fluxes to the wafer for neutrals and ions computed by the reactor model SEMS for both stove top and side coil configurations are shown in Fig. 4. The fluxes for Cl and Cl_2 are relatively uniform across the wafer for both configurations, as seen in Fig. 4(a). The dominant neutral is atomic chlorine, as Cl_2 is highly dissociated in the plasma. The ion fluxes, however, vary significantly with radial position (see Fig. 4(b)). For the stove top coil case, the Cl^+ flux decreases at outer radii, because the peak in the Cl^+ density occurs mid-radius and drops off at larger radii. Although the Cl_2^+ flux remains relatively constant over the wafer, its magnitude is approximately one-half that of Cl^+. The total ion flux is still small compared to the total neutral flux (for both coil configurations), which means that etching is accomplished in the "ion starved" regime, where the amount of ion flux dictates the etch rate. Therefore one would expect that the spatial non-uniformity of the ion flux would lead to lower etch rates at larger radii for the stove top coil case. However, the opposite scenario is true for the side coil reactor. In this case, both Cl^+ and Cl_2^+ fluxes increase with increasing radii due to the peak ion densities close to the coils. At 15 cm, the total ion flux to the wafer ($Cl^+ + Cl_2^+$) is higher for the side coil case compared with the fluxes at ~3 cm, due to the high ionization near the outer coils. This in turn will lead to higher etch rates at larger radii.

The ambipolar electric fields calculated from SEMS are shown in Fig. 5. Note that these are the fields in the presheath; the figures do not include the fields in the sheath for clarity, as the sheath fields are orders of magnitude higher. The electric fields are relatively small in the middle of the reactor but become quite large near the walls. In Fig. 5(a), the electric fields above the wafer at small radii ($R < 10$ cm) are nearly perpendicular and fairly uniform. However, due to

the stove top coil configuration, at larger radii, the electric fields are pointed toward the outer walls. This leads to ions being accelerated in the presheath in the $+\theta$ direction. Overall, the fields above the wafer are uniform in the stove top configuration. However, as seen in Fig. 5(b), the side coil reactor generates electric fields which are primarily non-perpendicular to the substrate. For $R < 2$ cm, the electric fields are nearly perpendicular, but become steeper in angle for larger radii. The magnitude of the electric fields at larger radii are smaller, however, due to the location of the coils on the outer wall. Since the field lines point toward the center of the reactor above the wafer, ions are accelerated in the $-\theta$ direction.

Typical distribution functions of Cl_2^+ and Cl on the wafer at $R = 7.32630$ cm are shown in Fig. 5. The distribution functions are calculated from PICNIC and are normalized from Eq. 4 from raw counts of particles as they land at specified locations. The distributions at different radial locations across the wafer do not qualitatively vary in a significant fashion. The velocity and angular distribution functions (VADF) are for the side coil case, although the VADFs for the stove top coil case are qualitatively the same. The recorded velocity of the species when it hits the wafer is actually the velocity magnitude, with the impacting angled defined as in Eq. 3. The VADF for Cl_2^+, as shown in Fig. 5(a), is very narrow in angular range. The ions gain energy in the axial direction due to the electric field in the sheath. This increase in axial velocity is usually far greater than the thermal ion speed, which leads to a tight distribution as the sheath is assumed to be collisionless. The average impacting velocity corresponds to roughly 23 eV. In contrast, the VADF for Cl in Fig. 5(b) covers a broad range of angles and represents an isotropic distribution on the surface, or a cosine dependence on impacting angle. The VADF is broadened by the momentum transfer collisions with Cl and Cl_2. The VADF has the expected Maxwellian dependence with velocity and a cosine distribution with angle. Because these cases do not

consider gas flow effects, the number of Cl_2 particles generated and collected on the wafer in PICNIC is small and statistics are poor. Hence for input into SPELS, we assume that Cl_2 has the same cosine dependence as Cl but is normalized to the bulk fluxes calulated in SEMS (shown in Fig. 4).

The velocity dependence of the distribution functions (such as those shown in Fig. 5) can be eliminated by integration. This resulting function is the net flux as a function of impacting angle,

$$g(\theta) = \frac{\int f(v,\theta) \cdot v^2 dv}{\iint f(v,\theta) \cdot v^2 dv \cdot \cos\theta \, d\theta}. \qquad [9]$$

The degree to which the distributions $f(v,\theta)$ are skewed can be determined by plotting g as a function of angle. These integrated values of g are shown in Figs. 7 and 8. For the stove top coil configuration in Fig. 7, both Cl_2^+ and Cl^+ ions impact the wafer at nearly head-on incidence at almost all radii. However, at R = 14.8080 cm, the flux $g(Cl^+)$ shows a distinct shift to the positive angle direction and is not centered at zero incidence. Although the amount of shift is small (~ 2.4°), the resulting etch profiles are sensitive to the ion distributions and will reflect this skew. The increase in the flux of ions that are directed with $\theta > 0$ indicates that at these larger radii, more ions have a directed velocity from the bulk plasma toward the outer wall. In other words, as the ions strike the wafer, their energy is directed toward the sidewall due to acceleration from the center of the plasma. This is due to the peak ion density being located mid-reactor, and is reflected in the electric field vector plot shown in Fig. 5(a). The Cl^+ ions demonstrate the same off-axis shift at large radii, as seen in Fig. 7(b). In contrast, the shift in

angular flux for the side coil case occurs in the $\theta < 0$ direction, as shown in Fig. 8. This time, ions are accelerated away from the sidewall and toward the center of the plasma, due to the ion peak densities being located near the sidewalls. Again, the ambipolar electric fields above the wafer show that the ions are accelerated in the $-\theta$ direction upon entering the sheath. The distributions for both Cl and Cl_2^+ are shifted by 3 to 5°. One surprising aspect is that the ion distributions are slightly less skewed at larger radii. This is because even though the electric fields have steeper angles at larger radii, the field magnitudes are smaller, so that the ions gain less angular energy in the presheath.

These calculated VADFs are then used to calculate the flux at each point in the trench in SPELS. For the following profiles, we assume a normalizing length of $L = 0.5$ μm and a hard mask thickness of 0.4 L. The trench opening is equivalent to L. The trench evolution is given for every 0.1 of the total simulation time. All other conditions are equivalent to those given in Ref. 17. The profiles at different radial locations are shown in Figs. 9 and 10. For the stove top coil case, all simulations are run for the same amount of time. This time corresponds to the amount of time it takes to etch a depth of L in open space at $R = 7.3263$ cm. All trenches are tapered in shape, again indicating that the plasma is in the ion-starved regime. The fluxes of Cl and Cl_2 are high ($\sim 10^{17}$ cm^{-2} s^{-1}) and are relatively constant with radius, as seen in Fig. 4. The flux of Cl_2^+ is also fairly constant over the wafer. However, the flux of Cl^+ decreases with increasing radius, leading to an overall decrease in etch depth versus radial location. The profile at $R = 14.8080$ cm also has a slight slant to the right. This is consistent with the skew in the ion fluxes in the positive θ direction. With more ions directed toward the right (or $\theta > 0$), etching should increase toward the right side. The difference in etched depth at the center of the trench at the outer location is approximately 16% less than at 2.81780 cm.

The profiles from the side coil reactor are shown in Fig. 10. As for the stove top coil cases, these simulations were run for the time it takes to etch a depth of L at R = 7.3263 cm. The plasma non-uniformities are reflected in the resulting profiles. Again, the profiles are tapered in shape as were the profiles for the stove top coil case. All of the profiles have a slant toward the left, which is due to the shift of the ion fluxes in the $\theta < 0$ direction. This shift is due to the peak ion densities occurring near the sidewall coils, with the ions gaining directed energy in the $-\theta$ direction in the presheath. The ions are not accelerated perpendicularly, but at a slight angle to the left, leading to increased etching at an angle. For the side coil cases, the neutral fluxes at larger radii increase slightly, whereas the ion fluxes increase dramatically as shown in Fig. 4. This increase in the ion flux leads to an overall increase in etch rate with increasing radius, which is the opposite trend for the stove top coil case. The difference in the etched depths is 57% (R = 2.81780 vs. 14.8080 cm), which is far greater than for the stove top coil configuration. Clearly, the plasma non-uniformities for fluxes and electric fields create dramatic differences in the etched profiles across the wafer. These small shifts in the ion VADFs that cause a skew in the etched profiles have been observed experimentally. For example, the features etched in pure chlorine plasmas by Lane *et al.*,[22] as well as those of Bogart *et al.*,[23] have the same qualitative tilting. It is worth noting that the trenches depicted in these references have straight sidewalls with no bowing, but both sidewalls are parallel and tilted, relative to the bottom plane.

IV. Concluding Remarks

A set of models, ranging from reactor-level to wafer-scale in domain size, was integrated to simulate etching profile evolution. These models calculate the fluxes of neutrals and ions as a

function of velocity and angle impacting the wafer. Our approach includes a continuum based plasma code and a PIC simulation to generate distribution functions. A level set code, SPELS, calculates the resulting profiles based on the fluxes generated from SEMS and PICNIC. Although such distributions were calculated using these specific simulations, SPELS is a stand-alone code that can use data generated from other models and codes. In the present work, we have used these suite of simulators to study etch profiles in chlorine etching of silicon in inductively coupled plasma reactors. No specific experiments have been modeled as complete sets of experimental conditions along with detailed results are not available in the literature. Nevertheless, we have conducted this study in the spirit of similar, model-only studies of etching, including angular distribution calculations and profile simulations.[3,16,24,25,26,27,28,29]

The most influential aspect on the etch profiles for these reactor geometries is the location of the peak of the ion densities. The location of the peak affects the total (bulk) flux of the ions to the surface versus radial location, and also controls the amount of skew, if any, that the impacting ions have. For the stove top coil configuration, the peak occurs at mid-reactor and causes a shift in the ion distribution function. Although the amount of shift is small, the etch rate is sensitive to the angular distribution and the effect is quite pronounced at larger radii. For the side coil cases, the peak in the ion densities occurs at outer radii, near the coils. The ion fluxes are less uniform across the wafer, and the distributions have a noticeable shift toward negative angles. The etching profiles all are slanted and the variations in the etch depth are significantly greater than for the stove top coil case. Thus, the uniformity of the entire plasma can impact the uniformity of the etched profiles. Such geometric concerns can determine the amount of center-to-edge differences across the substrate and the amount of skew in profiles at the wafer edge.

V. Acknowledgments

DB's work was performed under NASA contract NAS2-99092 to Eloret.

Table 1. Electron impact reactions used in SEMS. Rates are taken from Ref. 21.

Reaction	Type	Rate (cm^3/s) (T_e in eV)
$e + Cl_2 \rightarrow Cl_2^+ + e + e$	Ionization	$2.12802 \times 10^{-8}\ T_e^{0.771} \exp(-11.7/T_e)$
$e + Cl_2 \rightarrow Cl + Cl + e$	Dissociation	$3.99000 \times 10^{-8}\ T_e^{0.115} \exp(-4.43/T_e)$
$e + Cl_2 \rightarrow Cl_2 + e$	E. Exc. B3p	$1.22999 \times 10^{-7}\ T_e^{1.12} \exp(-4.3/T_e)$
$e + Cl_2 \rightarrow Cl_2 + e$	E. Exc. 21p and 21s	$9.4999 \times 10^{-9}\ T_e^{0.861} \exp(-9.0/T_e)$
$e + Cl_2 \rightarrow Cl_2 + e$	Vibrational	$3.1400 \times 10^{-8}\ T_e^{1.41} \exp(-1.35/T_e)$
$e + Cl \rightarrow Cl + e$	E. Exc. 4s	$1.2700 \times 10^{-8} \exp(-10.97/T_e)$
$e + Cl \rightarrow Cl + e$	E. Exc. 4p	$4.7900 \times 10^{-8} \exp(-10.29/T_e)$
$e + Cl \rightarrow Cl + e$	E. Exc. 3d	$1.9900 \times 10^{-8} \exp(-10.06/T_e)$
$e + Cl \rightarrow Cl + e$	E. Exc. 5p	$9.3200 \times 10^{-9} \exp(-11.06/T_e)$
$e + Cl \rightarrow Cl + e$	E. Exc. 4d	$9.2000 \times 10^{-9} \exp(-11.15/T_e)$
$e + Cl \rightarrow Cl + e$	E. Exc. 5d	$5.2000 \times 10^{-9} \exp(-11.12/T_e)$
$e + Cl \rightarrow Cl^+ + 2e$	Ionization	$2.9600 \times 10^{-8}\ T_e^{0.554} \exp(-13.1/T_e)$
$e + Cl_2 \rightarrow Cl^- + Cl$	Diss. attach.	1.0000×10^{-10}
$e + Cl_2^+ \rightarrow Cl + Cl$		$9.6793 \times 10^{-8}\ T_e^{-0.61} \exp(1.82 \times 10^{-6}/T_e)$
$e + Cl^- \rightarrow Cl + 2e$		$2.9455 \times 10^{-8}\ T_e^{0.68} \exp(-3.8/T_e)$

Table 2. Estimated heavy particle reactions used in PICNIC.

Reaction	k (cm^3/s)	σ_0 (cm^2)
$Cl^- + Cl^+ \rightarrow Cl + Cl$	5.00×10^{-8}	
$Cl^- + Cl_2^+ \rightarrow Cl + Cl_2$	5.00×10^{-8}	
$Cl + Cl + M \rightarrow Cl_2 + M$	6.74×10^{-32} (cm^6/s)	
$Cl^+ + Cl_2 \rightarrow Cl + Cl_2^+$		1.00×10^{-15}
$Cl^+ + Cl \rightarrow Cl + Cl^+$		1.00×10^{-15}
$Cl^- + Cl \rightarrow Cl + Cl^-$		1.00×10^{-15}
$Cl_2^+ + Cl_2 \rightarrow Cl_2 + Cl_2^+$		4.40×10^{-15}

Figure Captions

Fig. 1. The etching geometry is a two dimensional rectangular trench in silicon with a hard mask layer. Ions and neutrals impact the substrate at an angle θ with respect to the vertical. Particles landing with $\theta < 0$ have an angle "to the left", and those with $\theta > 0$ land "to the right." The normal to the interface or level set at each point is denoted by $\hat{n}$, and its angle with respect to the vertical is defined as ξ.

Fig. 2. Ion density contours for Cl_2^+ and Cl^+ in a stove top coil ICP as computed by the fluid model. Peaks for both ion densities occur mid-reactor and close to the coils.

Fig. 3. Ion density contours for Cl_2^+ and Cl^+ in a side coil ICP. Peaks occur near the sidewalls, and both densities are comparable in scale.

Fig. 4. Fluxes from the plasma to the wafer as a function of radial location for stove top and side coil cases. Fluxes are calculated from SEMS. (a) Cl and Cl_2, and (b) Cl^+ and Cl_2^+.

Fig. 5. Electric field vectors for (a) stove top and (b) side coil reactors. Electric fields in the presheath are more uniform above the wafer for the stove top configuration, whereas the fields in the side coil reactor have sharp angles (but lower magnitudes) at larger radii.

Fig. 6. Velocity and angular distribution functions (VADFs) for (a) Cl_2^+ and (b) Cl, at R = 7.32630 cm in a side coil ICP. Ion distributions are tightly centered, whereas the neutral distributions are broad and have a cosine dependence indicating isotropy.

Fig. 7. Integrated ion fluxes as a function of impact angle, stove top coil configuration. Integrating g over θ yields the net flux. Integrated fluxes for (a) Cl_2^+ and (b) Cl^+. Note the shift toward positive angles for R = 14.8080 cm.

Fig. 8. Integrated ion fluxes as a function of impact angle, side coil configuration. Fluxes shown are for (a) Cl_2^+ and (b) Cl^+. All fluxes are peaked at negative angles, ranging from 3-5° off center.

Fig. 9. Etching profiles for the stove top coil configuration at different radial locations. Locations are at (a) 2.81780 cm, (b) 7.32630 cm, and (c) 14.8080 cm. The skewed profile in (c) reflects the shift in the ion angular fluxes shown in Fig. 7.

Fig. 10. Etching profiles for the side coil configuration at (a) 2.81780 cm, (b) 7.32630 cm, and (c) 14.8080 cm. All three profiles are skewed toward the left, which is due to the shift in the ion angular fluxes toward negative angles.

References

[1] M. A. Vyvoda, H. Lee, M. V. Malyshev, F. P. Klemens, M. Cerullo, V. M. Donnelly, D. B. Graves, A. Kornblit, and J. T. C. Lee, "Effects of plasma conditions on the shapes of features etched in Cl_2 and HBr plasmas. I. Bulk crystalline silicon etching," *J. Vac. Sci. Technol. A*, vol. 16, no. 6, pp. 3247-3258, 1998.

[2] J.-H. Lee, G.-Y. Yeom, J.-W. Lee, and J.-Y. Lee, "Study of shallow silicon trench etch process using planar inductively coupled plasmas," *J. Vac. Sci. Technol. A*, vol. 15, no. 3, pp. 573-578, 1997.

[3] M. Tuda, K. Nishikawa, and K. Ono, "Numerical study of the etch anisotropy in low-pressure, high-density plasma etching," *J. Appl. Phys.*, vol. 81, no. 2, pp. 960-967, 1997.

[4] K. H. A. Bogart and V. M. Donnelly, "On the constant composition and thickness of the chlorinated silicon surface layer subjected to increasing etching product concentrations during chlorine plasma etching," *J. Appl. Phys.*, vol. 86, no. 4, pp. 1822-1833, 1999.

[5] N. Layadi, V. M. Donnelly, and J. T. C. Lee, "Cl_2 plasma etching of Si(100): Nature of the chlorinated surface layer studied by angle-resolved x-ray photoelectron spectroscopy," *J. Appl. Phys.*, vol. 81, no. 10, pp. 6738-6748, 1997.

[6] B. A. Helmer and D. B. Graves, "Molecular dynamics simulation of Cl_2^+ impacts onto a chlorinated silicon surface: Energies and angles of the reflected Cl_2 and Cl fragments," *J. Vac. Sci. Technol. A*, vol. 17, no. 5, pp. 2759-2770, 1999.

[7] D. E. Hanson, J. D. Kress, and A. F. Voter, "Reactive ion etching of Si by Cl and Cl_2 ions: Molecular dynamics simulations with comparisons to experiment," *J. Vac. Sci. Technol. A*, vol. 17, no. 4, pp. 1510-1513, 1999.

[8] M. Balooch, M. Moalem, W.-E. Wang, and A. V. Hamza, "Low-energy Ar ion-induced and chlorine ion etching of silicon," *J. Vac. Sci. Technol. A*, vol. 14, no. 1, pp. 229-233, 1996.

[9] J. P. Chang and H. H. Sawin, "Kinetic study of low energy ion-enhanced polysilicon etching using Cl, Cl_2, and Cl^+ beam scattering," *J. Vac. Sci. Technol. A*, vol. 15, no. 3, pp. 610-615, 1997.

[10] A. P. Mahorowala and H. H. Sawin, "Etching of polysilicon in inductively coupled Cl_2 and HBr discharges. III. Photoresist mask faceting, sidewall deposition, and microtrenching," *J. Vac. Sci. Technol. B*, vol. 20, no. 3, pp. 1077-1083, 2002.

[11] D. Bose, T. R. Govindan, and M. Meyyappan, "A continuum model for the inductively coupled plasma reactor in semiconductor processing," *J. Electrochem. Soc.*, vol. 146, no. 7, pp. 2705-2711, 1999.

[12] J. A. Levinson, E. S. G. Shaqfeh, M. Balooch, and A. V. Hamza, "Ion-assisted etching and profile development of silicon in molecular and atomic chlorine," *J. Vac. Sci. Technol. B*, vol. 18, no. 1, pp. 172-190, 2000.

[13] H. H. Hwang and M. J. Kushner, "Ion energy distributions in radio frequency discharges sustained in gas mixtures obtained using a Monte Carlo-fluid hybrid model: endothermic processes and ion holes," *Plasma Sources Sci. Technol.*, vol. 3, no. 2, pp. 190-205, 1994.

[14] D. P. Lymberopoulos and D. J. Economou, "Two-dimensional simulation of polysilicon etching with chlorine in a high density plasma reactor," *IEEE Trans. Plasma Sci.*, vol. 23, no. 4, pp. 573-580, 1995.

[15] M. A. Lieberman and A. J. Lichtenberg, *Principles of Plasma Discharges and Materials Processing*. New York: Wiley, 1994, pp. 157-158.

[16] R. J. Hoekstra and M. J. Kushner, "Predictions of ion energy distributions and radical fluxes in radio frequency biased inductively coupled plasma etching reactors," *J. Appl. Phys.*, vol. 79, no. 5, pp. 2275-2286, 1996.

[17] H. H. Hwang, T. R. Govindan, and M. Meyyappan, "Feature profile evolution simulation using a level set method," *J. Electrochem. Soc.*, vol. 146, no. 5, pp. 1889-1894, 1999.

[18] H. H. Hwang, M. Meyyappan, G. S. Mathad, R. Ranade, "Simulations and experiments of etching of silicon in HBr plasmas for high aspect ratio features," *J. Vac. Sci. Technol. B*, accepted for publication in Nov./Dec. 2002.

[19] J. A. Sethian, *Level Set Methods*. Cambridge, England: Cambridge University Press, 1996, pp. 15-21.

[20] J. Y. Choe, I. P. Herman, and V. M. Donnelly, "Analysis of the etching of silicon in an inductively coupled chlorine plasma using laser thermal desorption," *J. Vac. Sci. Technol. A*, vol. 15, pp. 3024-3031, 1997.

[21] L. G. Christophorou and J. K. Olthoff, "Electron interactions with Cl_2," *J. Phys. Chem. Ref. Data*, vol. 28, no. 1, pp. 131-169, 1999.

[22] J. M. Lane, F. P. Klemens, M. V. Malyshev, and J. T. C. Lee, "Feature evolution during plasma etching. II. Polycrystalline silicon etching," *J. Vac. Sci. Technol. A*, vol. 18, pp. 188-196, 2002.

[23] K. H. Bogart, F. P. Klemens, M. V. Malyshev, J. I. Colonell, V. M. Donnelly, J. T. C. Lee, and J. M. Lane, "Mask charging and profile evolution during chlorine plasma etching of silicon," *J. Vac. Sci. Technol. A*, vol. 18, no. 1, pp. 197-206, 2000.

[24] T. J. Cotler, M. S. Barnes, and M. E. Elta, "A Monte Carlo microtopography for investingating plasma/reaction ion etch profile evolution," *J. Vac. Sci. Technol. B*, vol. 6, no. 2, pp. 542-550, 1988.

[25] I. V. Katardjiev, G. Carter, M. J. Nobes, S. Berg, and H.-O. Blom, "Three-dimensional simulation of surface evolution during growth and erosion," *J. Vac. Sci. Technol. A*, vol. 12, no. 1, pp. 61-68,1994.

[26] S. Hamaguchi and M. Dalvie, "Microprofile simulations for plasma etching with surface passivation," *J. Vac. Sci. Technol. A*, vol. 12, no. 5, pp. 2745-2753, 1994.

[27] S. D. Athavale and D. J. Economou, "Molecular dynamics simulation of atomic layer etching of silicon," *J. Vac. Sci. Technol. A*, vol. 13, no. 3, pp. 966-971, 1995.

[28] R. J. Hoekstra, M. J. Grapperhaus, and M. J. Kushner, "Integrated plasma equipment model for polysilicon etch profiles in an inductively coupled plasma reactor with subwafer and superwafer topography," *J. Vac. Sci. Technol. A*, vol. 15, no. 4, pp. 1913-1921, 1997.

[29] T. Panagopoulos and D. J. Economou, "Plasma sheath model and ion energy distribution for all radio frequencies," *J. Appl. Phys.*, vol. 85, no. 7, pp. 3435-3443, 1999.

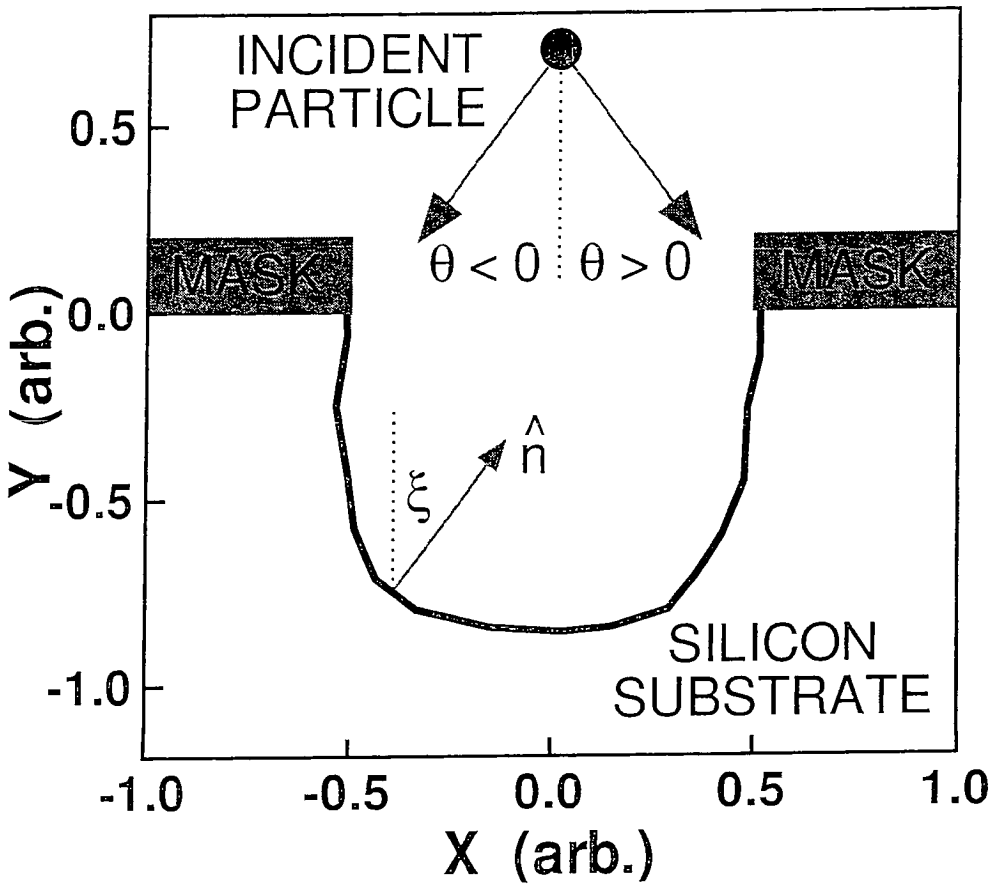
INCIDENT
PARTICLE
MASK
MASK
θ < 0
θ > 0
ξ
n̂
SILICON
SUBSTRATE
0.5
0.0
-0.5
-1.0
Y (arb.)
-1.0
-0.5
0.0
0.5
1.0
X (arb.)

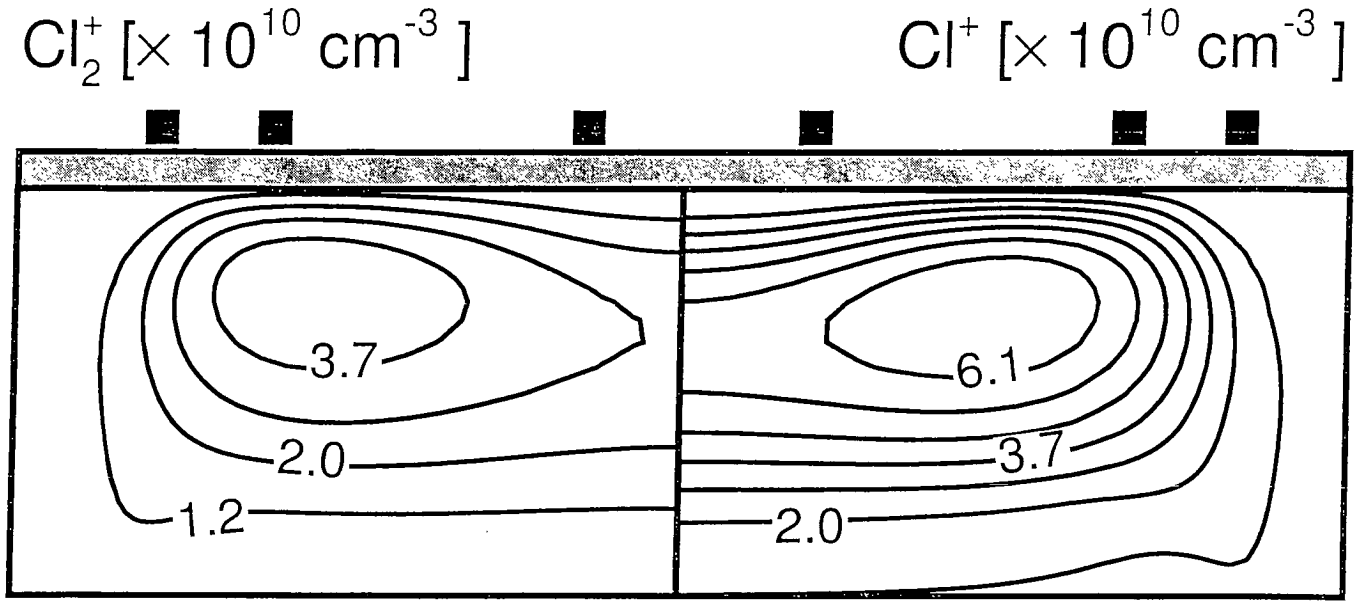
Cl_2^+ [× 10^{10} cm^{-3}]
Cl^+ [× 10^{10} cm^{-3}]
3.7
2.0
1.2
6.1
3.7
2.0

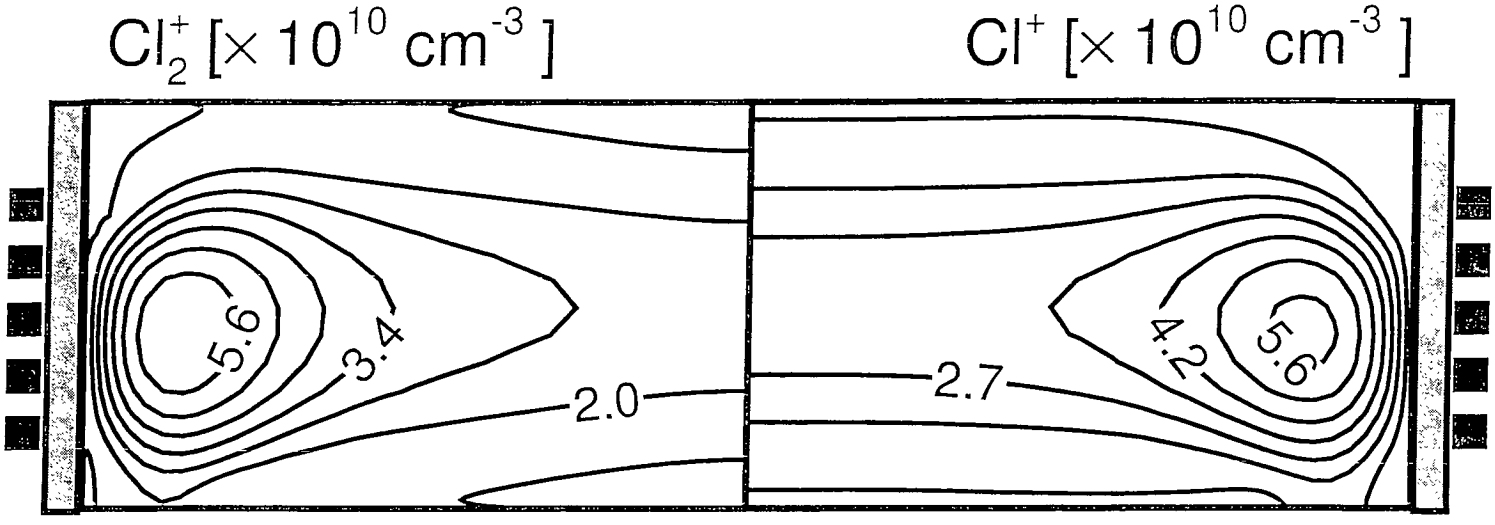

Hwang et al.

(a)

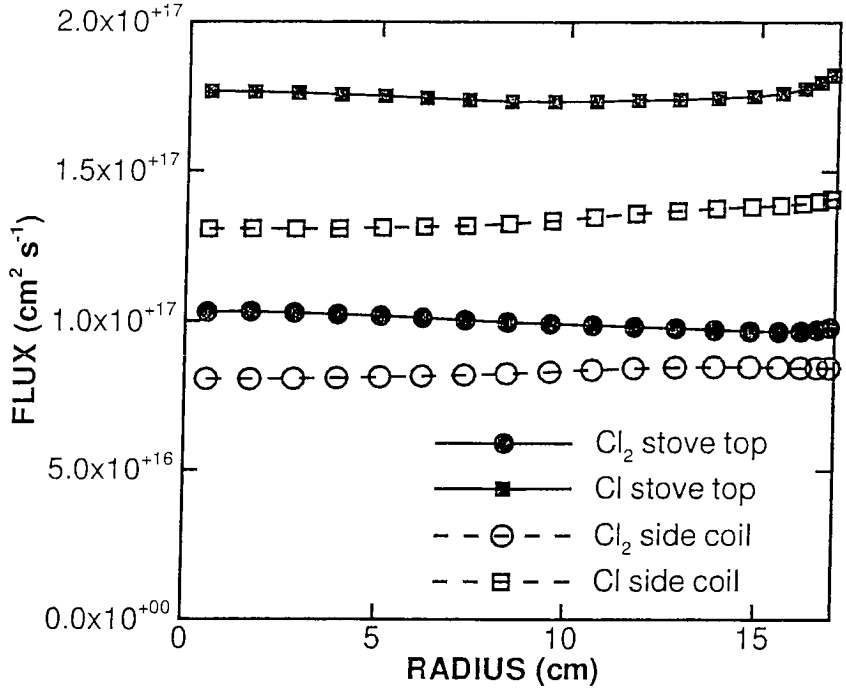
2.0x10+17
1.5x10+17
1.0x10+17
5.0x10+16
0.0x10+00
FLUX (cm2 s-1)
0
5
10
15
RADIUS (cm)
Cl2 stove top
Cl stove top
Cl2 side coil
Cl side coil

(b)

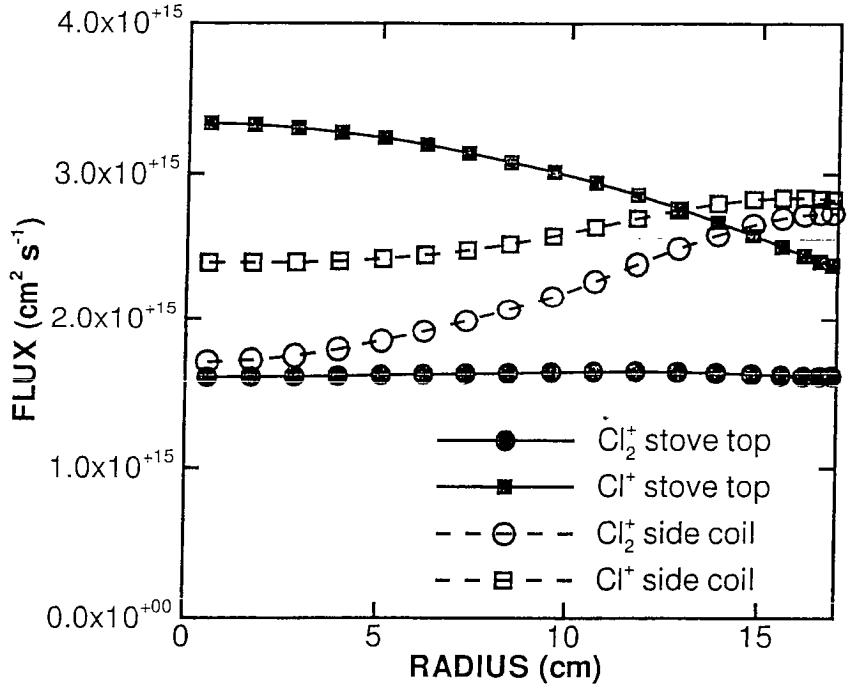
4.0x10+15
3.0x10+15
2.0x10+15
1.0x10+15
0.0x10+00
FLUX (cm2 s-1)
0
5
10
15
RADIUS (cm)
Cl2+ stove top
Cl+ stove top
Cl2+ side coil
Cl+ side coil

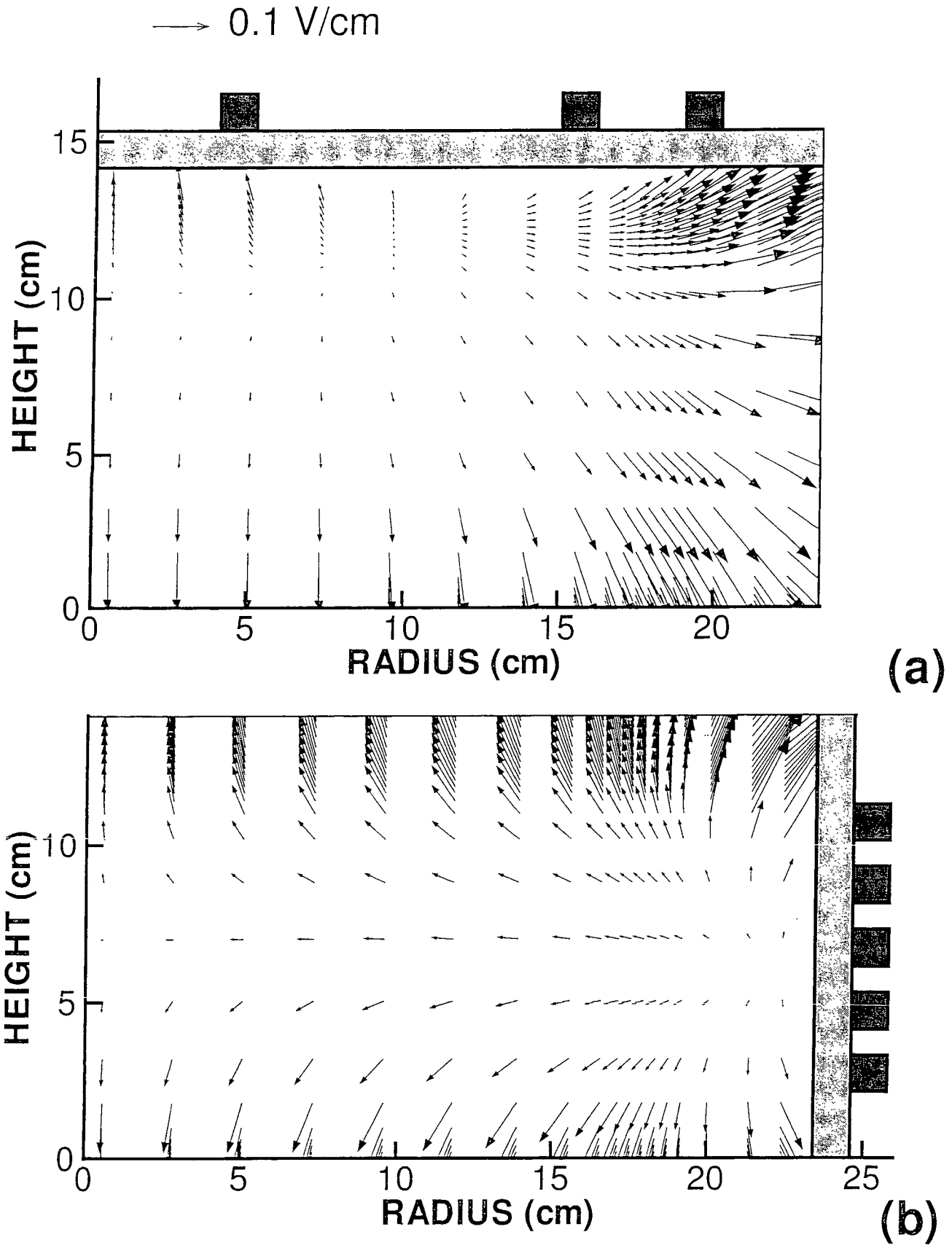

Hwang et al.

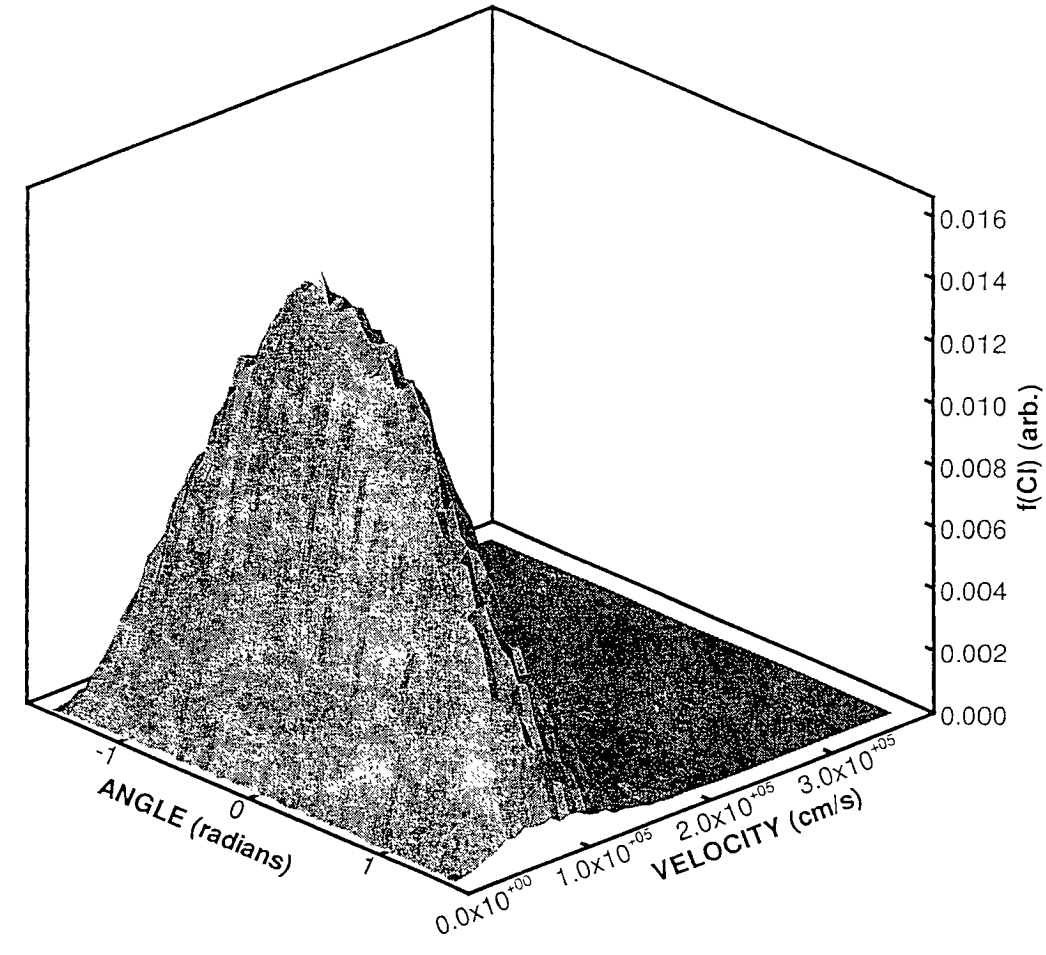

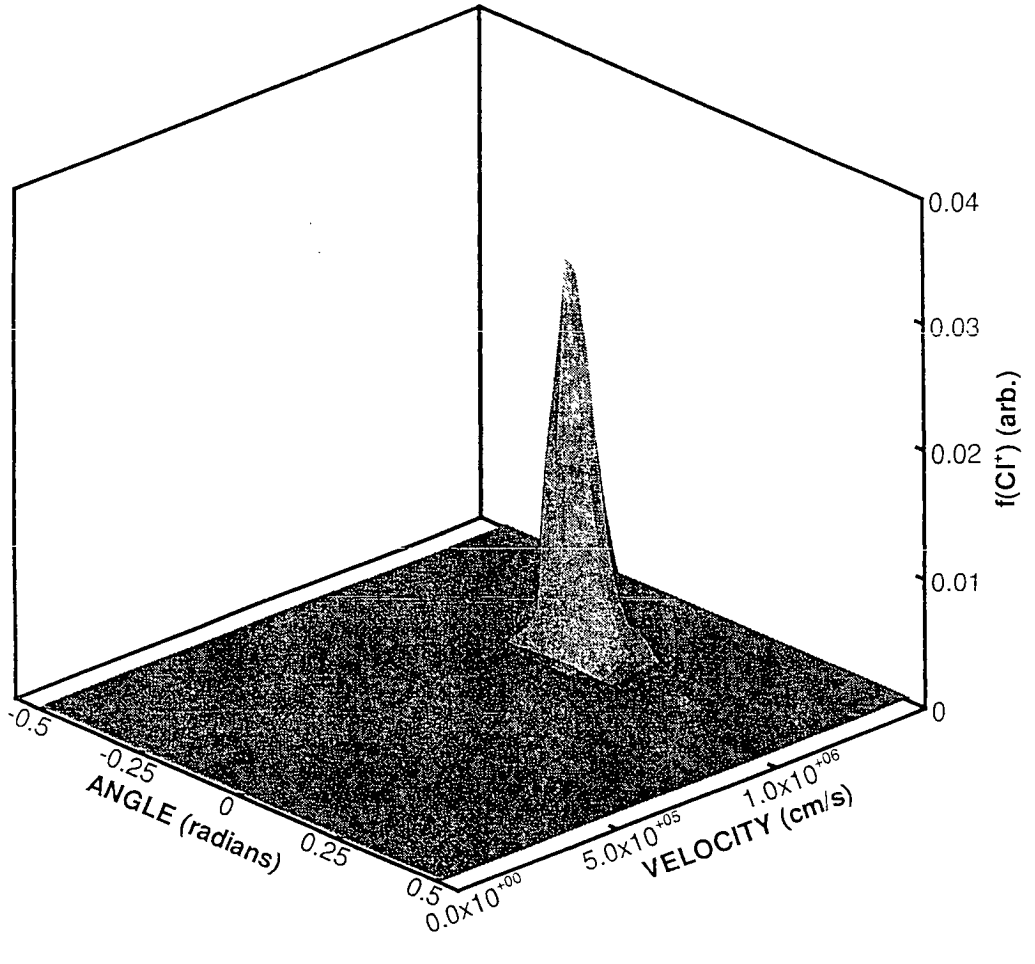

Hwang et al.
Figure 6 of 10

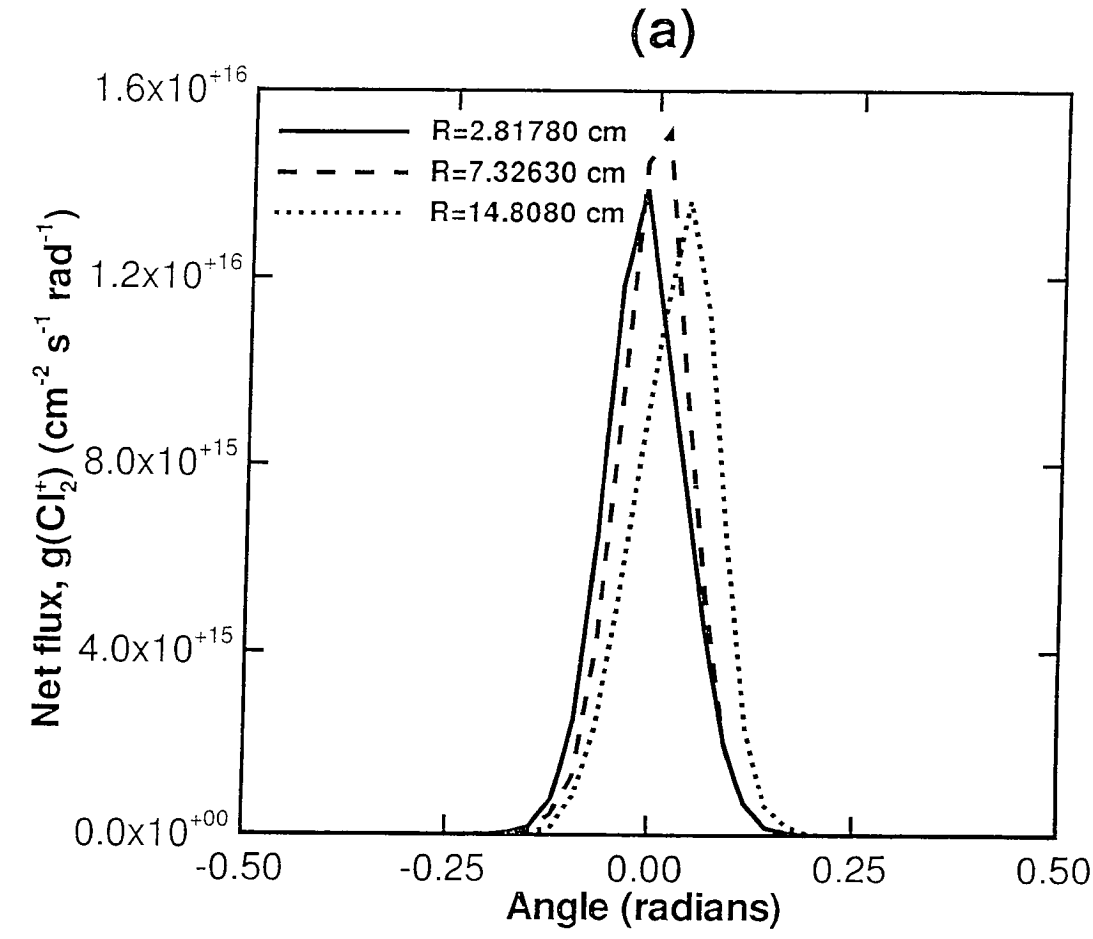
(a)
1.6x10+16
1.2x10+16
8.0x10+15
4.0x10+15
0.0x10+00
Net flux, g(Cl2+) (cm-2 s-1 rad-1)
R=2.81780 cm
R=7.32630 cm
R=14.8080 cm
-0.50
-0.25
0.00
0.25
0.50
Angle (radians)

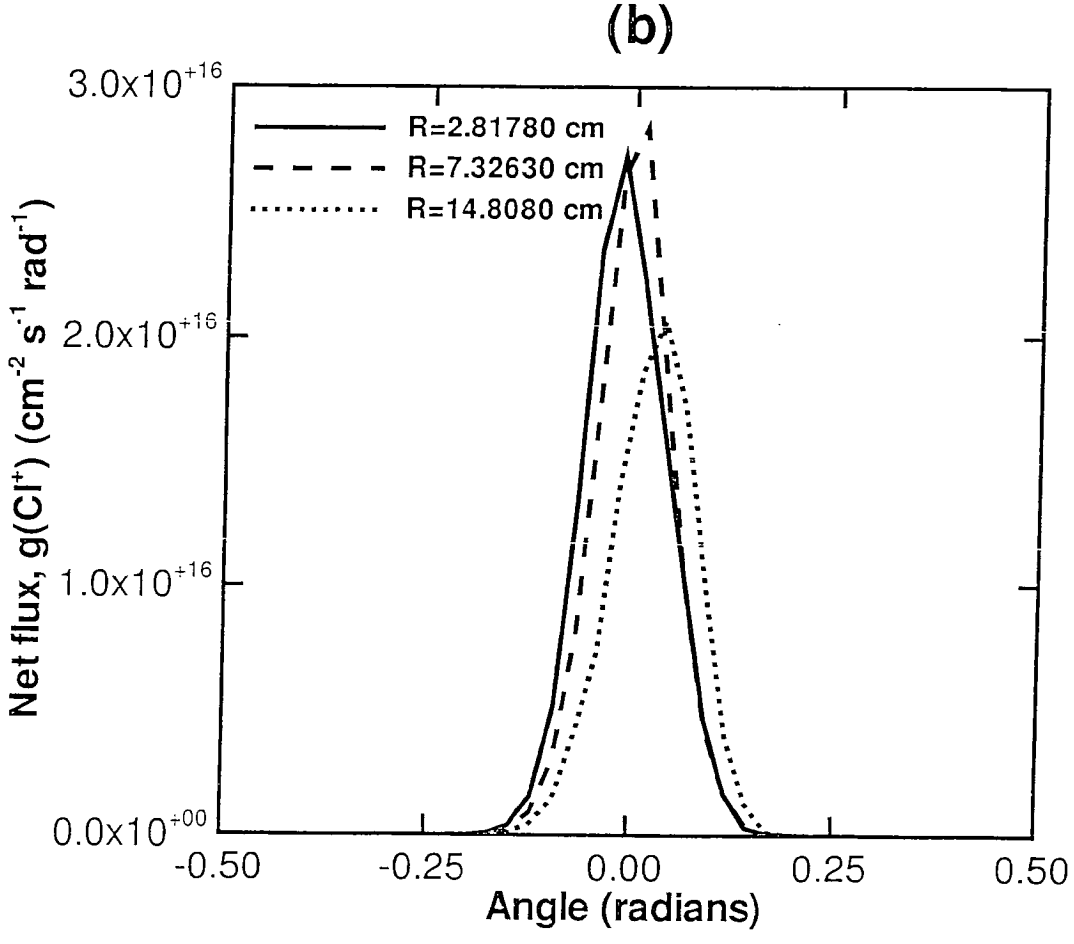
(b)
3.0x10+16
2.0x10+16
1.0x10+16
0.0x10+00
Net flux, g(Cl+) (cm-2 s-1 rad-1)
R=2.81780 cm
R=7.32630 cm
R=14.8080 cm
-0.50
-0.25
0.00
0.25
0.50
Angle (radians)

Hwang et al.

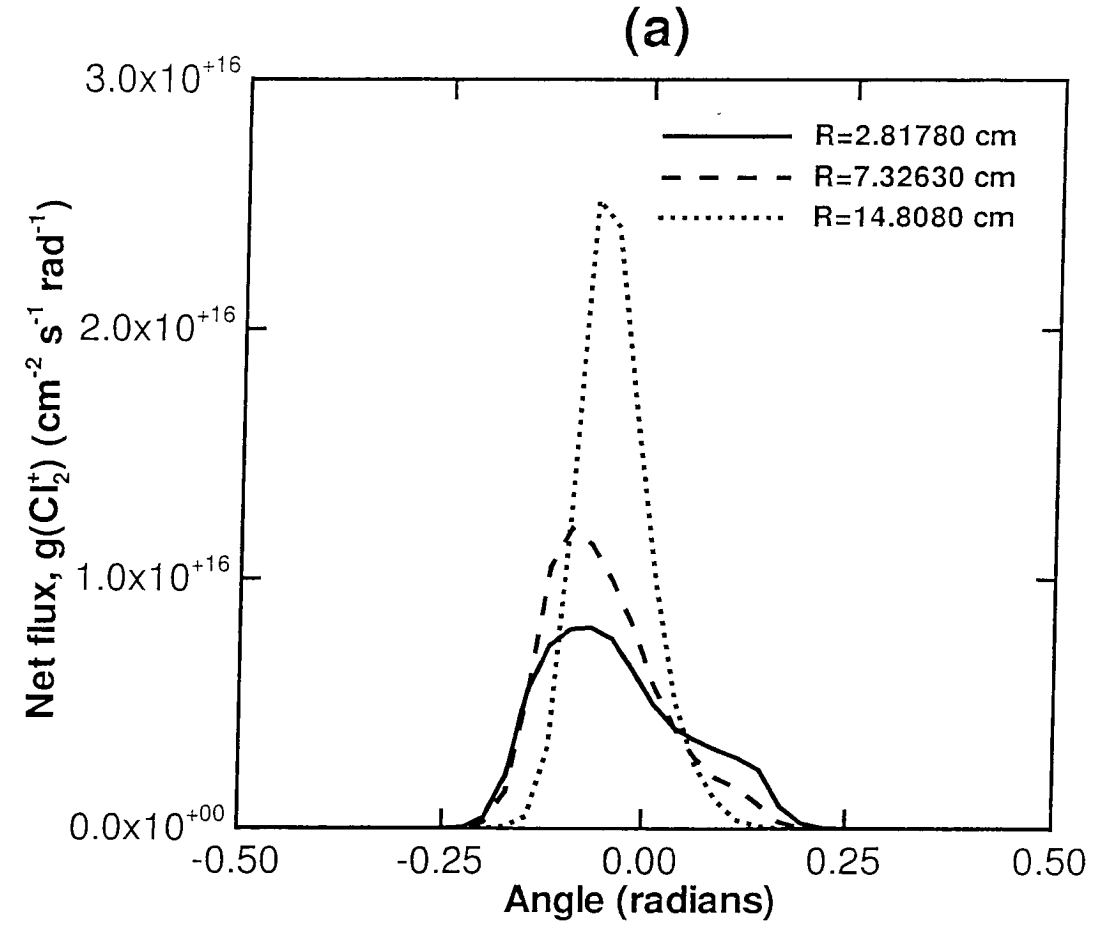
(a)
3.0x10+16
2.0x10+16
1.0x10+16
0.0x10+00
Net flux, g(Cl2+) (cm-2 s-1 rad-1)
R=2.81780 cm
R=7.32630 cm
R=14.8080 cm
-0.50
-0.25
0.00
0.25
0.50
Angle (radians)

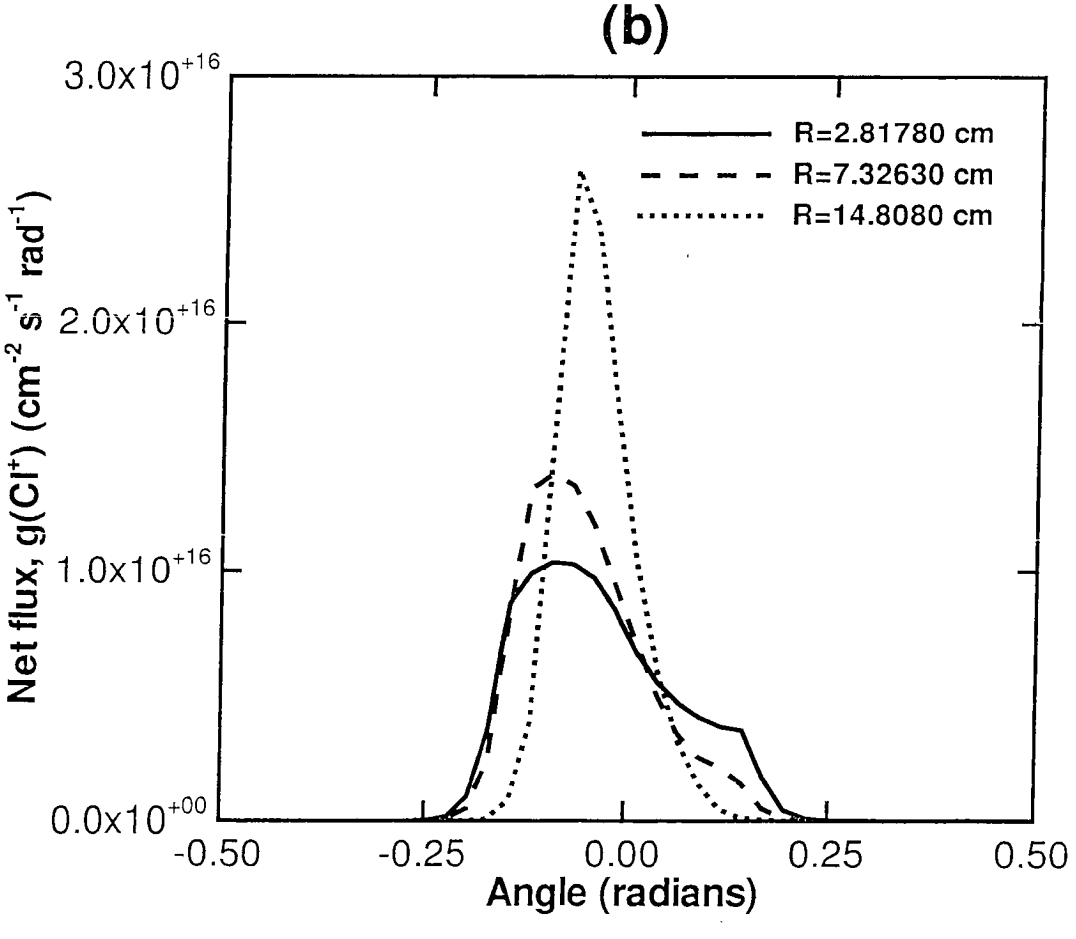
(b)
3.0x10+16
2.0x10+16
1.0x10+16
0.0x10+00
Net flux, g(Cl+) (cm-2 s-1 rad-1)
R=2.81780 cm
R=7.32630 cm
R=14.8080 cm
-0.50
-0.25
0.00
0.25
0.50
Angle (radians)

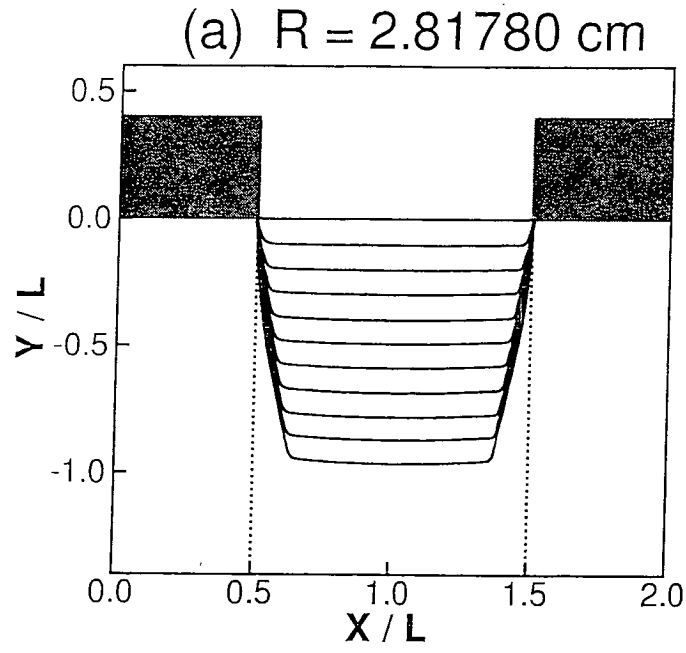
(a) R = 2.81780 cm
0.5
0.0
-0.5
-1.0
Y / L
0.0
0.5
1.0
1.5
2.0
X / L

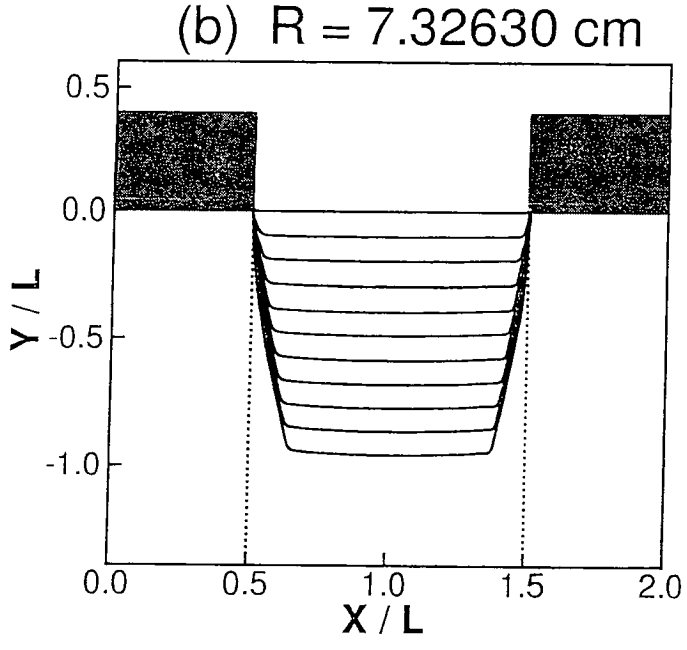
(b) R = 7.32630 cm
0.5
0.0
-0.5
-1.0
Y / L
0.0
0.5
1.0
1.5
2.0
X / L

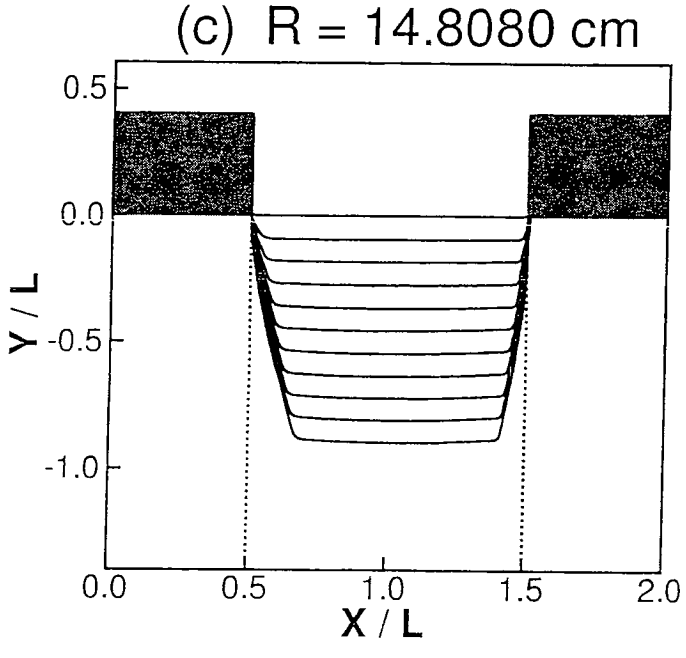
(c) R = 14.8080 cm
0.5
0.0
-0.5
-1.0
Y / L
0.0
0.5
1.0
1.5
2.0
X / L

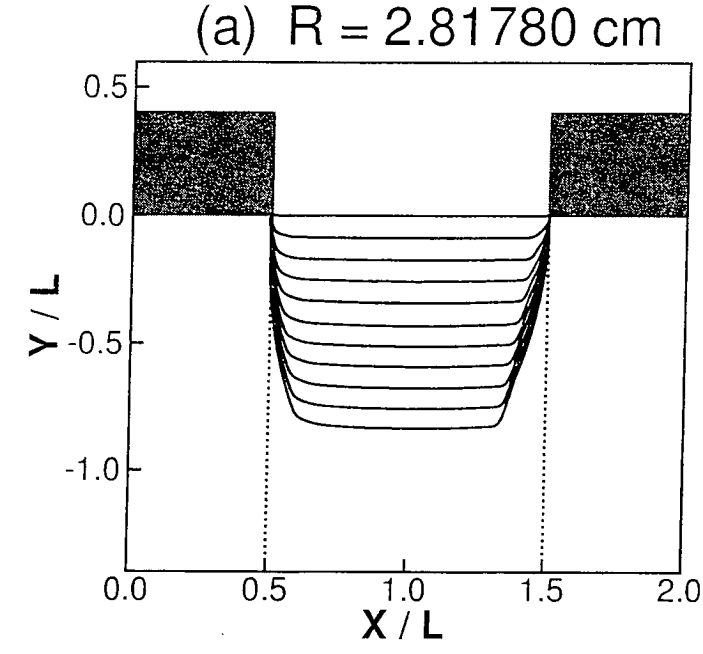

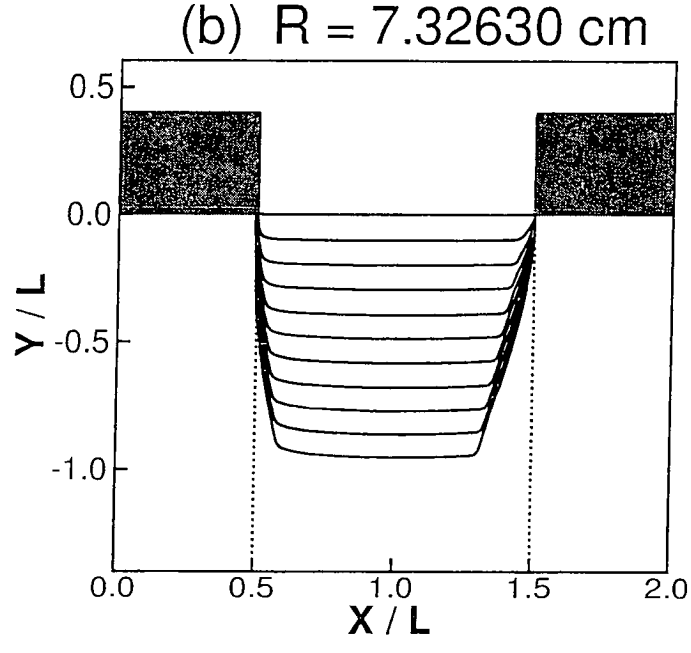

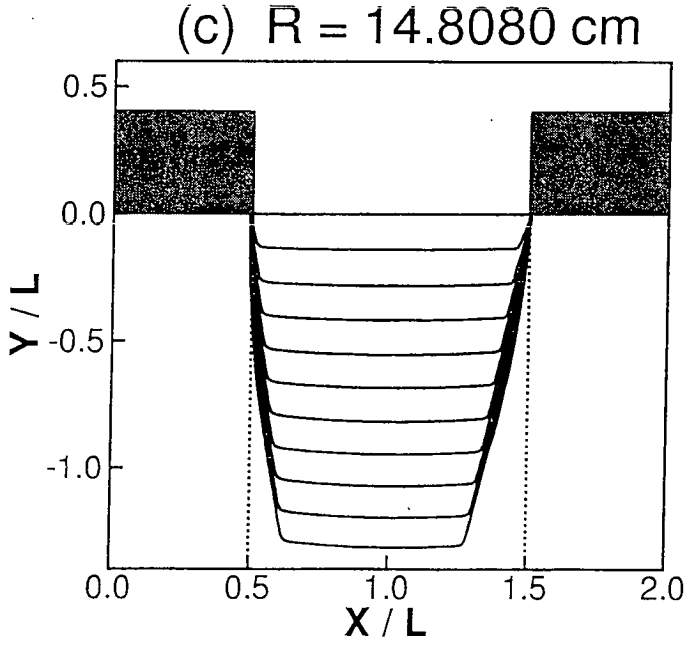

Hwang et al.
Fig. 10 of 10